Catalysis Science & Technology

Accepted Manuscript

This article can be cited before page numbers have been issued, to do this please use: Y. Shimoyama, S. Tamura, Y. Kitagawa, D. Hong and Y. Kon, *Catal. Sci. Technol.*, 2020, DOI: 10.1039/D0CY01758B.

ROYAL SOCIETY OF CHEMISTRY

rsc.li/catalysis

View Article Online
DOI: 10.1039/D0CY01758B

ARTICLE

A cobalt-substituted Keggin-type polyoxometalate for catalysis of oxidative aromatic cracking reactions in water

Received 00th January 20xx,
Accepted 00th January 20xx

DOI: 10.1039/x0xx00000x

Yoshihiro Shimoyama,[a] Satoru Tamura,[b] Yasutaka Kitagawa,[c] Dachao Hong,*[a,d] and Yoshihiro Kon[a,d]

Efficient detoxification of harmful benzene rings into useful carboxylic acids in water is indispensable for achieving a clean water environment. We report herein that oxidative aromatic cracking (OAC) reactions in water were archived by the catalytic system using a cobalt-substituted Keggin-type polyoxometalate (**Co-POM**) as a catalyst, Oxone® monopersulfate compound as a sacrificial oxidant and sodium bicarbonate as an additive under mild conditions. Sodium bicarbonate plays a crucial role in the selective OAC reactions by **Co-POM** using ethylbenzenesulfonate as a model substrate. The reactive species was characterized to be a cobalt(III)-oxyl species based on ^{31}P NMR, UV-vis spectroscopic, kinetic, and theoretical analyses. The electrophilicity of the cobalt(III)-oxyl species was demonstrated by a linear relationship with a negative slope in the Hammett plots of initial rates obtained from the OAC reactions of *m*-xylenesulfonate derivatives. Besides, we have verified the degradation pathway of the OAC reactions using benzene as a model substrate in the catalytic system. The degradation was initiated by an electrophilic attack of the cobalt(III)-oxyl species on benzene to yield phenol followed by producing catechol, muconic acid, maleic/fumaric acid, tartaric acid derivatives and formic acid on the basis of ^{1}H NMR spectroscopic analysis.

Introduction

Aromatic compounds such as benzene have been widely used as primary raw materials for industrial production of their derivatives and synthetic resins.[1] In these compounds, benzene, polychlorinated biphenyls (PCBs) and polyaromatic hydrocarbons (PAHs) have been strictly restricted for their waste management due to their carcinogenicity, noxiousness and teratogenicity.[2] As these compounds are highly stable by virtue of their resonance stabilization and strong chemical bonding,[3] oxidative aromatic cracking (OAC) reactions by dioxygen requires high temperatures and results in massive emission of CO_2,[4,5] which has caused greenhouse effect impacting on environmental issues and industrial benefits.[6] Therefore, conversing the aromatics into valuable compounds under mild conditions has been exploited. For example, *in-situ* formed ruthenium(VIII) tetraoxide ($Ru^{VIII}O_4$) by sodium periodate ($NaIO_4$) as an oxidant has been reported so far in catalytic oxidation of aromatics under mild conditions.[7,8] However, these reactions require toxic halogen-containing oxidants and solvents such as $NaIO_4$ and CCl_4. It remains challenging to crack harmful aromatics into useful carboxylic acids in environmentally benign systems under mild conditions.[9]

Recently, Kojima et al. have reported an oxidative cracking of benzene rings to afford carboxylic acids in water using a ruthenium(II) complex having a *N*-heterocyclic carbene (NHC) ligand as a catalyst (Scheme 1).[10] In this reaction, a cerium(IV) oxidant with excess amounts was used to generate a ruthenium(III)-oxyl (Ru^{III}-O•) species[11] that exhibits selective catalytic hydroxylation of aromatic compounds. However, a reactive species such as metal-bound oxyl-radical or high-valent metal-oxo species formed in the catalytic OAC reactions can also oxidize organic aromatic ligands themselves, resulting in the degradation of metal complexes with organic ligands.[10,12] Thus, oxidative-tolerant ligands such as inorganic metal oxide anions are required to develop efficient catalysts for OAC reactions. Furthermore, metal complex catalysts using earth-abundant metal ions are desired to apply in practical reactions.

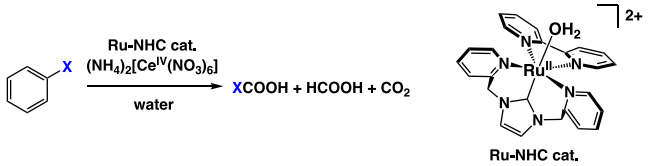

Scheme 1 Catalytic cracking of benzene rings by Ru(II)-NHC catalyst.[10]

Polyoxometalates (POMs) composed of metal oxide anions are known as highly durable materials toward oxidation.[13] Several types of polyoxometalates were reported to be efficient

[a] Interdisciplinary Research Center for Catalytic Chemistry, National Institute of Advanced Industrial Science and Technology (AIST), 1-1-1 Higashi, Tsukuba, Ibaraki 305-8565, Japan. E-mail: hong-d@asit.go.jp (D.H)
[b] Institute for Energy and Material/Food Resources, Technology Innovation Division, Panasonic Corporation, 1006 Kadoma, Kadoma City, Osaka 571-8508, Japan.
[c] Department of Materials Engineering Science, Graduate School of Engineering Science, Osaka University, 1-1 Machikaneyama-cho, Toyonaka, Osaka 560-8531, Japan
[d] Global Zero Emission Research Center, National Institute of Advanced Industrial Science and Technology (AIST), 1-1-1 Higashi, Tsukuba, Ibaraki 305-8565, Japan.
Electronic Supplementary Information (ESI) available: [NMR and UV-vis spectra, electrochemical measurements, table and time profiles of products and Cartesian coordinates of Co(III) oxyl species]. See DOI: 10.1039/x0xx00000x

catalysts for oxidation reactions.[14,15] Foreign metal ions are introduced into metal oxide anions of POMs as M-substituted POMs in which M acts as a reactive centre. For example, cobalt-substituted Keggin-type POMs have been studied as water oxidation catalysts in water.[16-18] The reactive species of cobalt-substituted POMs have been proposed as cobalt-oxyl or cobalt-oxo species in the water oxidation. In this context, cobalt-substituted POMs can be promising catalysts toward OAC reactions. However, there has been no report so far on cobalt-substituted POMs as catalysts for OAC reactions, and the reaction mechanism of OAC reactions by cobalt-substituted POMs has yet to be clarified.

We report herein that a monocobalt-substituted Keggin-type polyoxometalate ($K_5[PCo(OH_2)W_{11}O_{39}]$, **Co-POM**) acts an efficient catalyst for OAC reactions using Oxone® as an environmentally benign oxidant and bicarbonate salts as additives in water. The mechanistic insights into the OAC reactions by **Co-POM** in water were revealed based on NMR, UV-vis spectroscopic, kinetic, and theoretical analyses.

Results and Discussion

The catalyst of **Co-POM** was prepared according to a literature procedure[19] and characterised by ^{31}P NMR, UV-vis and FT-IR measurements (Fig. S1).[17,20] A solo peak at 465 ppm derived from **Co-POM** was observed in the ^{31}P NMR spectra, indicating the single product without any impurities. Additionally, UV-vis and FT-IR spectra were also exhibited a characteristic band at 530 nm and 800–1100 cm^{-1}, respectively, which are consistent with the reported spectra.[17,20] The electrochemical measurements of **Co-POM** in water were also performed, as showed in Fig. S2, in which an irreversible oxidation wave at +1.45 V (*vs.* Ag/AgCl) is assigned to the oxidation potential of Co(II) centre, and reversible redox waves at –0.85 and –1.04 V can be derived from redox of W ions.[20b] We have employed the prepared **Co-POM** as a catalyst for OAC reactions as below.

The catalytic OAC reactions were performed in D_2O containing sodium 4-ethylbenzenesulfonate (EtBnS) as a substrate, **Co-POM** as a catalyst, Oxone® monopersulfate compound ($KHSO_4{\cdot}K_2SO_4{\cdot}2KHSO_5$) as a sacrificial oxidant and sodium bicarbonate as an additive. The products obtained in the reactions were quantified by ^{1}H NMR spectroscopic analyses. We have observed phenylethanol derivative (**1**), acetophenone derivative (**2**), acetic acid (**3**), formic acid (**4**), and propionic acid (**5**) as the products in the ^{1}H NMR spectra of the reaction solution after 24 h (Scheme 2, Fig. S3).[21] The turnover number (TON) and product concentrations for these products are shown in Table 1 (see also Table S1 for the TONs of all products). To distinguish between benzylic oxidation and aromatic oxidation (OAC reactions), we utilize A/B ratios that are defined as [**5**]/([**1**]+[**2**]+[**3**]) in the catalytic EtBnS oxidation reactions. As the source of formic acid can be derived from both benzylic oxidation and aromatic oxidation, it was excluded from the calculation of A/B ratios to avoid overestimation. Acetic acid can be produced in the benzylic oxidation through Baeyer-Villiger oxidation[22] of **2** by Oxone® to yield 4-acetoxybenzenesulfonate followed by its hydrolysis rather than the OAC reactions by an electrophilic attack of Co-oxyl species to the aromatic ring of **2** having electron-withdrawing groups (sulfonate and acetyl) (Fig. S4). Thus, we categorized acetic acid as B in the reactions. The catalytic oxidation of EtBnS by **Co-POM** has afforded propionic acid as a major product with A/B ratio of 1.08, indicating the aromatic oxidation was primarily catalysed by **Co-POM** with a TON of 31 (entry 1). The TON for **Co-POM** has been achieved to 498 under optimized conditions with 5.0 μM **Co-POM**. In the absence of sodium bicarbonate, benzylic oxidation predominantly took place in the catalytic EtBnS oxidation by **Co-POM**, resulting in the decrease of A/B ratio to 0.18 (entry 2). Sodium bicarbonate plays an essential role in the selective aromatic oxidation of EtBnS by **Co-POM**. Sodium bicarbonate is used to stabilize **Co-POM** by buffering pH within 5–8 in water because the reaction solutions acidified by Oxone® result in the hydrolysis of **Co-POM** in the absence of 1.0 M sodium bicarbonate (*vide infra*).

Several control experiments were performed to support the superiority of **Co-POM** as an effective catalyst for the selective

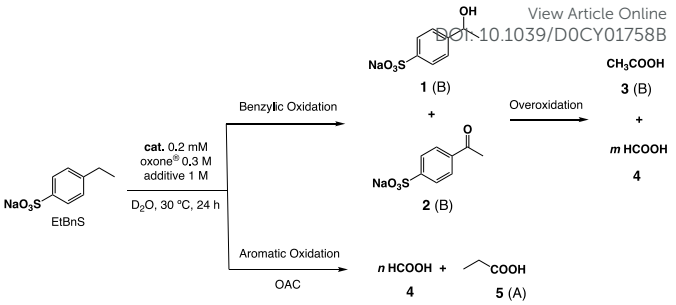

Scheme 2 Schematic representation of catalytic oxidation of EtBnS in this work.

Table 1 TONs and A/B ratio of the product obtained from the catalytic OAC reactions [a]

Entry	Catalyst	TON (Yield, %) [b]		A/B ratio [c]
		A (= [**5**])	B (= [**1** + **2** + **3**])	
1	**Co-POM**	31 (6.1)	29 (5.7)	1.08
2	**Co-POM** [d]	20 (4.0)	113 (22.5)	0.18
3	–	– (0.3)	– (2.5)	0.12
4	$Co^{II}(ClO_4)_2$	4 (0.9)	79 (15.6)	0.06
5	$H_3[PW_{12}O_{40}]$	2 (0.4)	12 (2.2)	0.18
6	$Co^{II}(ClO_4)_2$ + $H_3[PW_{12}O_{40}]$	7 (1.4)	58 (11.6)	0.12
7	$Co^{II}Cl_2$ + Na_2WO_4 + Na_2HPO_4	8 (1.5)	60 (11.9)	0.13
8 [e]	Ru(II)-NHC [f]	6 (1.3)	73 (15.1)	0.09

[a] Conditions: [Catalyst] = 0.20 mM, [$NaHCO_3$] = 1.0 M, [EtBnS] = 0.10 M, [Oxone®] = 0.30 M, Temp. = 30 °C, Solvent: D_2O (1.0 mL), reaction time: 24 h. [b] TON = [product]/[catalyst], Yield = ([product]/[EtBnS]) × 100. [c] A/B ratio = [**5**]/([**1**]+[**2**]+[**3**]). [d] No additive. [e] [Ru(II)-NHC] = 0.20 mM, $[(NH_4)_2Ce^{IV}(NO_3)_6]$ = 0.10 M, [EtBnS] = 0.10 M, Temp.: 30 °C, Solvent: D_2O, reaction time: 24 h. [f] Ru(II)-NHC catalyst was synthesized according to the previous literature.[10]

aromatic oxidation in the catalytic oxidation of EtBnS. (entries 3–7). Only trace amounts of products were observed without a **Co-POM** catalyst in the reaction solution (entry 3). When **Co-POM** was replaced with cobalt(II) perchlorate salt (entry 4)[23] or well-known Keggin-type phosphotungstic acid ($H_3[PW_{12}O_{40}]$) (entry 5), almost no aromatic oxidation was observed in the catalytic oxidation of EtBnS. The result denied the possibility that dissociated Co(II) ions from **Co-POM** act as catalysts for the aromatic oxidation. Besides, the use of both cobalt(II) perchlorate and $H_3[PW_{12}O_{40}]$, or the use of all of cobalt(II) chloride, $NaWO_4$ and Na_2HPO_4, which are the components of **Co-POM**, as catalysts afforded products oxidized at the benzylic position as a major product with low A/B ratios in the catalytic oxidation of EtBnS (entries 6–7). These results demonstrate that **Co-POM** in combination with sodium carbonate is indispensable for the aromatic oxidation in the catalytic oxidation of EtBnS and a sulfate or a persulfate radical derived from the oxidant should be ruled out as a reactive species.[24] Furthermore, the reactivity of **Co-POM** was compared to that of a reported catalytic system by a Ru(II)-NHC complex.[10] A low A/B ratio (0.09) for Ru(II)-NHC complex was observed in the catalytic oxidation of EtBnS (entry 8). It would be ascribed to a poor reactivity of Ru(III)-oxyl species, derived from the Ru(II)-NHC complex, to an electrophilic attack toward the aromatic ring of EtBnS. The reactivity of **Co-POM** is superior to that of the reported Ru(II)-NHC complex (TON = 6), although the TON comparison would not be fair because the reaction conditions in this work differ from the reported literature.

We have also examined the dependence of A/B ratios on reaction temperatures and concentrations of sodium bicarbonate and Oxone® in the catalytic oxidation of EtBnS by **Co-POM**. The A/B ratios were depressed in the increase of reaction temperatures (Fig. 1a). The A/B ratio was maximized at the concentration of 1.0 M sodium bicarbonate (Fig. 1b). The result can be attributed to the pH differences that strongly affect the stability of **Co-POM** in the reaction solutions. **Co-POM** is demonstrated to be hydrolyzed at a pH lower than 5 and higher than 8 (Fig. S5). In the absence of $NaHCO_3$, the pH with 0.30 M Oxone® remains to be 2 due to the acidification by Oxone®, resulting in the hydrolysis of **Co-POM**. On the other hand, the pH with 1.0 M $NaHCO_3$ has shifted to 8.8 in the absence of Oxone®. In addition, the plots of A/B ratios against Oxone® concentration showed a pseudo-volcano feature and a plateau region in the range from 0.15 M to 0.30 M was observed (Fig. 1c). Therefore, the optimized conditions in this work were determined to be 1.0 M $NaHCO_3$ and 0.30 M Oxone® (pH 5.9) operating at 30 °C for the catalytic reactions.

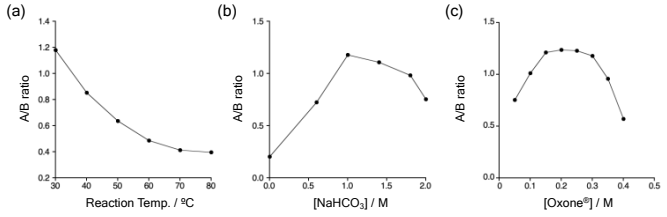

Fig. 1 Dependence of A/B ratio on (a) reaction temperatures and concentrations of (b) $NaHCO_3$ and (c) Oxone® in the OAC reactions of EtBnS by **Co-POM**. The reactions were performed in D_2O (1.0 mL) containing **Co-POM** (0.20 mM), $NaHCO_3$ (1.0 M), EtBnS (0.10 M) and Oxone® (0.30 M) at (a) 30–80 °C, (b) the concentrations of $NaHCO_3$ were varied from 0 to 2.0 M at 30 °C, and (c) the concentrations of Oxone® were varied from 0.050 to 0.40 M at 30 °C.

To reveal the mechanistic insights into the OAC reactions by **Co-POM**, we investigated UV-vis absorption changes in sub-stoichiometric or catalytic oxidation of EtBnS. UV-vis spectral titration upon addition of HSO_5^- to **Co-POM** was attempted to reveal intermediates of **Co-POM**. Highly broad absorption band around 400 – 900 nm has increased upon the addition of 3.0 mol equiv of HSO_5^- in the UV-vis spectral titration by HSO_5^- in water with sodium bicarbonate (Fig. 2a). The apparent colour of the solution turned brown during the rise of the broad absorption band. The absorption band with a characteristic peak at 495 nm was continuously raised by the addition of HSO_5^- up to 13 mol equiv of HSO_5^- (Fig. 2b). Meanwhile, the solution colour was changed to orange-brown. Besides, the similar absorption band was also observed in the catalytic reaction solutions without EtBnS at the initial reaction state and it was rapidly despaired by the addition of EtBnS (Fig. S6), indicating a plausible reactive species of **Co-POM** has been generated by HSO_5^-. When 10 mol equiv of EtBnS was added to the orange-brown solution (Figs. 2c and 2d), the characteristic absorption at 495 nm immediately decayed within 300 seconds to produce a pink species that was observed for the solution before the addition of HSO_5^-. The pink species suggest the regeneration of **Co-POM** as confirmed by ^{31}P NMR measurements together with the production of hydroxylated EtBnS (4-ethyl-3-hydroxy-benzene- sulfonate and 4-(1'-hydroxyethyl)-benzenesulfonate) as characterized by ^1H NMR and LC-MS measurements (Fig. S7).

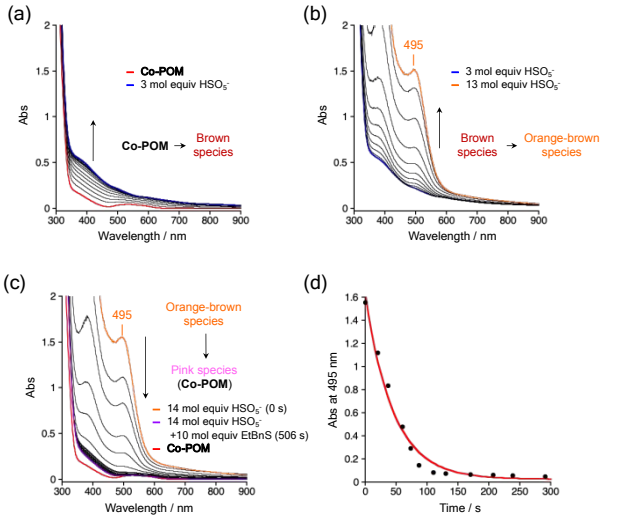

Fig. 2 UV-vis spectral titration upon addition of (a) 0 – 3.0 mol equiv. and (b) 3 – 13 mol equiv of Oxone® (HSO_5^-) into water containing $NaHCO_3$ (10 mM), Na_2SO_4 (50 mM) and **Co-POM** (1.0 mM) at RT. (c) UV-Vis absorption changes after an addition of EtBnS (10 mM) to the titration solution. (d) Time-profile of the absorbance at 495 nm for the solution of (c).

We attempted to characterize the reactive species (brown and orange-brown) based on paramagnetic ^{31}P NMR spectral

measurements in D_2O. A new diamagnetic ^{31}P NMR signal at +12.5 ppm was observed for the **Co-POM** solution upon addition of 3.0 mol equiv of HSO_5^- (Fig. S8a), supporting the formation of brown species in the UV-vis spectra (Fig. 2a). This signal can be assigned to a diamagnetic Co^{III} species, ($[PCo^{III}(HSO_5^-)W_{11}O_{39}]^{5-}$), that formed from 1e$^-$-oxidation of $[PCo^{II}(OH_2)W_{11}O_{39}]^{5-}$ followed by coordination of HSO_5^- to Co^{III} centre in a low-spin state (Scheme 3). It is reasonable to oxidase Co(II) of **Co-POM** to Co(III) by HSO_5^- based on the oxidation potential of Co(II) centre (E = +1.45 V vs Ag/AgCl) and the reduction potential of HSO_5^- (E > +1.6 V vs Ag/AgCl).[25] Excess HSO_5^- required for the experiments suggests that the formation of the diamagnetic Co^{III} species has an equilibrium between $[PCo^{III}(OH_2)W_{11}O_{39}]^{5-}$ and $[PCo^{III}(HSO_5^-)W_{11}O_{39}]^{5-}$. When further addition of HSO_5^- (14 mol equiv) into the solution, two paramagnetic ^{31}P NMR signals appeared at +54.7 ppm and +95.7 ppm (Fig. S8b). These paramagnetic species at +54.7 ppm and +95.7 ppm could be assigned to $[PCo^{III}(O\bullet)(W_{11}O_{39})]^{5-}$ (Co^{III}-oxyl) or $[PCo^{IV}(O)(W_{11}O_{39})]^{5-}$ (Co^{IV}-oxo) that represented as equivalent electronic structures.

Theoretical calculations on $[PCo(O)W_{11}O_{39}]^{5-}$ under vacuum have been conducted to distinguish whether Co^{III}-oxyl or Co^{IV}-oxo species are the dominant reactive species in the catalytic reaction by **Co-POM**. The optimized structures under doublet, quartet and sextet spin multiplicity are displayed in Fig. 3a.

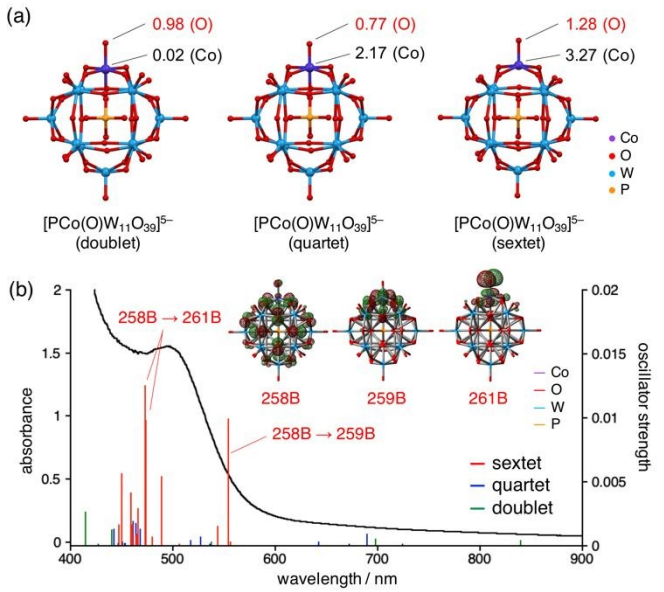

Fig. 3 (a) DFT-optimized structures, spin distributions and total energies of $[PCo(O)W_{11}O_{39}]^{5-}$ lying on doublet (left), quartet (centre) and sextet (right) spin multiplicity. (b) TD-DFT calculations for the optimized structures overlaid with an UV-vis absorption obtained from addition of 13 mol equiv. of HSO_5^- to **Co-POM** in water (see Fig. 2b). Inset shows the corresponding molecular orbitals (258B, 259B and 261B). All these calculations were conducted at the UB3LYP/LanL2TZ (W), 6-31G* (Co), 6-31+G* (O, P) level of theory.

Judging from the spin distribution of these optimized structures, the terminal oxygen coordinated to the Co centre with a spin density of approximately 1.0 indicates the oxyl-radical character of $[PCo(O)W_{11}O_{39}]^{5-}$ drawn as $[PCo^{III}(O\bullet)W_{11}O_{39}]^{5-}$. The structure with the sextet spin state was calculated to be the most stable among these optimized structures (Table S2). TD-DFT calculations show that the optimized structure with the sextet spin multiplicity gives good consistency in the observed absorption band of the orange-brown species with the peak at 495 nm, which is assigned to the ligand-to-metal charge transfer (LMCT) band of electron transition from 2p orbitals of bridging oxygen atoms (258B) to an anti-bonding orbital of Co-O bond (261B) (Fig. 3b). The oscillator strength at 554.19 nm is also attributed to the LMCT band of electron transition from 258B to Co d_π orbital (259B). Also, the cobalt(III)-oxyl species have been proposed as a reactive intermediate in catalytic oxidation reactions so far.[26-28] Thus, we conclude that the reactive orange-brown species is primarily derived from the Co^{III}-oxyl intermediate ($[PCo^{III}(O\bullet)W_{11}O_{39}]^{5-}$).

Based on the results of UV-vis spectral, ^{31}P NMR spectral measurements and theoretical calculations, we propose the reaction mechanism of sub-stoichiometric oxidation of EtBnS by **Co-POM** (Scheme 3) at the initial step. $[PCo^{II}(OH_2)W_{11}O_{39}]^{5-}$ is oxidized by HSO_5^- to generate $[PCo^{III}(OH_2)W_{11}O_{39}]^{4-}$ that is coordinated to HSO_5^- in the presence of excess HSO_5^- to form $[PCo^{III}(HSO_5^-)W_{11}O_{39}]^{5-}$. The Co^{III}-oxyl species, $[PCo^{III}(O\bullet)(W_{11}O_{39})]^{5-}$, formed from O–O cleavage of HSO_5^-,[29] reacts with EtBnS to produce hydroxylated EtBnS and regenerate $[PCo^{II}(OH_2)W_{11}O_{39}]^{5-}$.

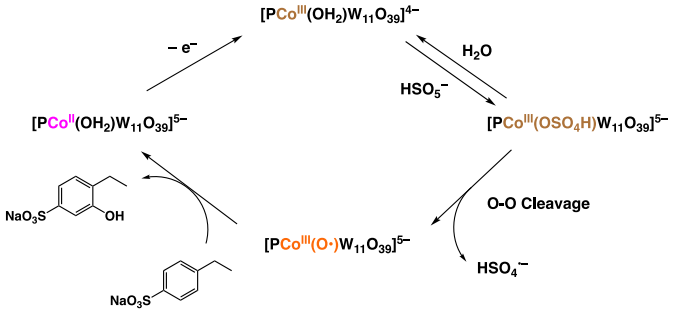

Scheme 3 Plausible reaction mechanism of sub-stoichiometric oxidation of EtBnS by **Co-POM**.

Kinetic analysis on the absorption decay of the Co^{III}-oxyl species was investigated to scrutinize a detailed reaction mechanism in the sub-stoichiometric oxidation by **Co-POM** using sodium *m*-xylenesulfonate (*m*XyS) as a standard substrate. We have employed *m*XyS as a substrate in order to synthesize its derivatives with facile methods. In the sub-stoichiometric oxidation of *m*XyS by **Co-POM**, the apparent rate constants (k_{obs}^H) for *m*XyS was determined to be 8.9×10^{-2} s^{-1} by fitting the absorption change at 495 nm based on pseudo-first-order kinetics (Fig. 4a). The rate constant (k_{obs}^D) for sodium trideuterated *m*-xylenesulfonate (*m*XyS-d_3) was obtained to be 6.3×10^{-2} s^{-1} (Fig. S9). A kinetic isotope effect (KIE = k_H/k_D) was calculated to be 1.4 in the sub-stoichiometric oxidation of *m*XyS by the Co^{III}-oxyl species. A KIE value of 1.7 was reported in oxidation reactions of benzene by hydroxyl radicals generated from H_2O_2, which was rationalized as the electrophilic attack of hydroxyl radicals on the aromatic ring of benzene.[30] Compared to the reported KIE value, the obtained KIE (1.4) demonstrates an electrophilic addition on the benzene ring of *m*XyS by the

View Article Online
DOI: 10.1039/D0CY01758B

Co^{III}-oxyl species. The results also suggest that the OAC reactions of EtBnS by **Co-POM** may undergo the step of electrophilic addition on the benzene ring by the Co^{III}-oxyl species. The sub-stoichiometric oxidation of monosubstituted *m*-xylenesulfonate (Y*m*XyS, Y = Br, NO_2) by **Co-POM** provides an apparent rate constant of 7.1×10^{-2} for BrXyS (k_{obs}^{Br}) and 6.2×10^{-2} s^{-1} for NO_2*m*XyS (k_{obs}^{NO2}) (Fig. 4b and 4c). The Hammett plots of the rate constants showed a linear relationship against Hammett parameters of substituents[31] with a negative slope (ρ = –0.5) in sub-stoichiometric oxidation of Y*m*XyS (Fig. 4d). The result also demonstrates that the OAC reactions by **Co-POM** took place *via* electrophilic addition on the aromatic ring of substrates by a Co^{III}-oxyl species, as mentioned above (Fig. 4e). Our results are consistent with reported catalytic OAC reactions of benzene by a Ru(II)-NHC complex[10] and a Cu complex[32] in which the reactive species are proposed as a Ru^{II}-oxyl (Ru^{III}-O•) and a Cu^{II}-oxyl (Cu^{II}-O•) species, respectively.

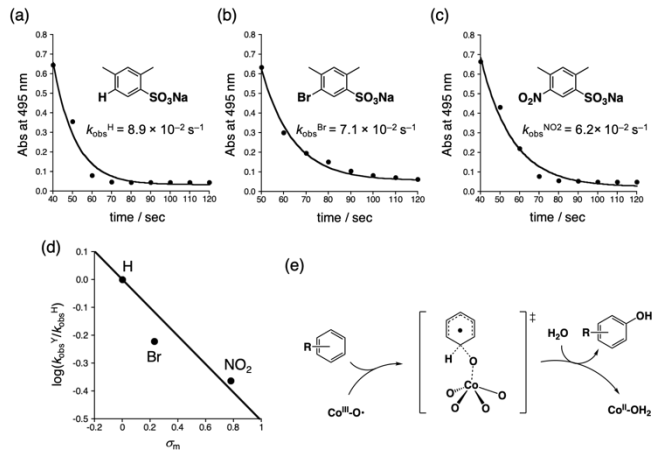

Fig. 4 (a) Time profiles of absorption decay of Co^{III}-oxyl species generated by the reaction of Oxone® ([HSO_5^-]: 14 mol eq.) and **Co-POM** in the oxidation of Y*m*XyS (Y = H, Br, NO_2). [**Co-POM**]: 1.0 mM, [Oxone®]: 7.0 mM ([HSO_5^-]: 14 mM), [Y*m*XyS]: 10 mM, [Na_2SO_4]: 50 mM, [$NaHCO_3$]: 10 mM, temp.: 25 °C. (b) Hammett plots on the apparent rate constant (k_{obs}) in the sub-stoichiometric oxidation of Y*m*XyS by **Co-POM**. (b) Schematic representation of benzene hydroxylation by the Co^{III}-oxyl (Co^{III}-O•) species.

We have also performed catalytic OAC reactions of benzene by **Co-POM** to reveal benzene degradation pathways by ^{1}H NMR spectra. While degradation pathways of benzene have been widely studied so far,[33] the degradation pathways by **Co-POM** has yet to be validated. In the catalytic OAC reactions of benzene by **Co-POM**, we observed several product peaks that are assigned to formic acid (8.4 ppm), phenol (around 7.0 ppm), maleic acid (6.5 ppm) and fumaric acid (6.0 ppm) by ^{1}H NMR spectra (Fig. S10 and Scheme 4). In the benzene oxidation, formic acid was observed as the primary oxidation product with a TON of 12 for **Co-POM** and a concentration of 2.4 mM based on ^{1}H NMR spectroscopic analysis. As phenol should be the first 2-electron oxidized intermediate among these products, we use phenol as a substrate to investigate the subsequent oxidation steps. Fig. S11a shows the ^{1}H NMR spectrum of the OAC reaction of phenol by **Co-POM**: formic acid, *cis*,*cis*-Muconic acid (***cc*MA**), muconolactone (**Mlac**), tetrahydrofuro[3,2-b]furan-2,5-dione (**Lac2**), and tartaric acid (**Tar**) were observed at 8.4 ppm, 7.8–6.3 ppm, 5.6 ppm, 5.5 ppm and 4.3 ppm, respectively, determined based on a reported literature.[34] When catechol or hydroquinone was employed as substrates in the OAC reactions, these characteristic peaks obtained using phenol as a substrate were also observed in the ^{1}H NMR spectra (Figs. S11b and S11c). The results suggest the primary degradation pathway in benzene oxidation should include phenol, catechol as oxidative intermediates. The production of formic acid was confirmed by the oxidation reactions using *trans*,*trans*-muconic acid (***tt*MA**), maleic acid (**Mal**) and tartaric acid (**Tar**) as substrates (Fig. S12). Therefore, the plausible degradation pathway of benzene by **Co-POM** in Scheme 4 is corroborated by the ^{1}H NMR spectral measurements.

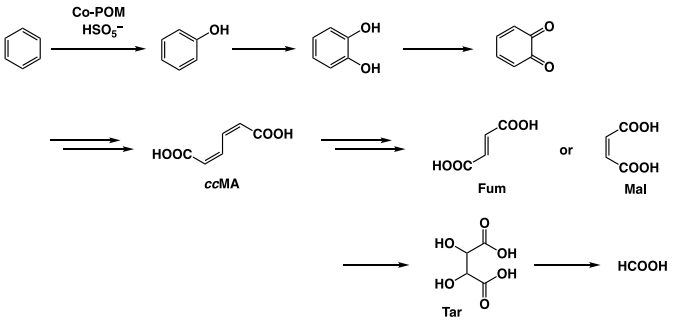

Scheme 4 plausible degradation pathway of the catalytic OAC reaction of benzene by **Co-POM**.

Conclusions

In summary, we have successfully constructed a catalytic system using **Co-POM** as a catalyst and Oxone® as an oxidant for environmentally benign OAC reactions of aromatic rings, which allows us to obtain useful carboxylic acids under mild conditions. In particular, oxidative cleavage of aromatic rings was executed dominantly in the presence of sodium bicarbonate as an additive in the catalytic system. The reactive species was characterized to be a cobalt(III)-oxyl species on the basis of control experiments, kinetic analysis, theoretical calculations, and UV-vis spectroscopic analysis. We demonstrate that aromatic substrates were oxidized by the cobalt(III)-oxyl species through an electrophilic addition on aromatic rings in the catalytic system. The degradation pathway of benzene in the catalytic system was verified by ^{1}H NMR spectral measurements in which phenol, catechol, and muconic acid derivatives were identified as oxidative intermediates. The catalytic oxidation using **Co-POM** as a catalyst and Oxone® as an oxidant can provide a fundamental understanding of the nature of cobalt(III)-oxyl species derived from **Co-POM** for selective oxidation reactions. Finally, this work offers valuable insights into OAC reactions by the **Co-POM** catalytic system toward the development of efficient catalysts for degradations of persistent organic pollutants into useful carboxylic acids in an environmentally benign manner.

Conflicts of interest

There are no conflicts to declare.

View Article Online
DOI: 10.1039/D0CY01758B

Acknowledgements

D.H. gratefully acknowledges support from the Japan Society for the Promotion of Science (JSPS) by the Leading Initiative for Excellent Young Researchers (LEADER). Y.S also gratefully acknowledges support from Grants-in-Aid (20K15328) from JSPS.

Experimental

General

^{1}H NMR spectral measurements were performed on JEOL JNM-ECX 400 spectrometer using 4,4-dimethyl-4-silapentanesulfonic acid sodium salt (DSS) as an internal standard. Paramagnetic ^{31}P NMR spectral measurements were performed on Bruker AVANCE HD 400 spectrometer. UV-Vis spectral measurements at RT were performed using SCINCO UV-visible spectrophotometer S-3100. LC-MS measurements were performed on SHIMADZU LCMS-2020 spectrometer. Purified water (18.2 MΩ cm) was obtained from a Milli-Q system (Direct-Q3 UV, Millipore). Electrochemical measurements are carried out using HZ-7000 HOKUTO DENKO.

Chemicals.

Sodium 4-ethylbenzenesulfonate (EtBnS) and sodium *m*-xylenesulfonate (*m*XyS) were purchased from Tokyo Chemical Industry Co., Ltd. Sodium bicarbonate and Oxone® monopersulfate compound were purchased from Fujifilm Wako Pure Chemical Corp. D_2O was purchased from ISOWATER Corp. NO_2*m*XyS,[35] and *m*XyS-d_3[10] were synthesized and characterized according to literature procedures. All chemicals and solvents were used without further purification.

General procedure for catalytic OAC reactions of EtBnS.

Oxone®, $NaHCO_3$, and EtBnS were dissolved into 1.0 mL of D_2O. **Co-POM** in D_2O solution was added to the mixture. The reaction mixture was stirred at 30 – 80 ℃. After each reaction time, 300 µL of the mixture was diluted with 300 µL of D_2O solution containing DSS as an internal standard. The total 600 µL solution was submitted to the ^{1}H NMR spectroscopic analysis. Benzene oxidation was performed in a mixed solution (D_2O : Benzene = 1: 0.2 (v/v)) containing Oxone®, $NaHCO_3$ and **Co-POM**.

UV-vis spectroscopic titration of Co-POM.

Aqueous solution of **Co-POM** (1.0 mM), $NaHCO_3$ (10 mM), Na_2SO_4 (50 mM) was titrated by aqueous solution of Oxone® at 25 ℃. Na_2SO_4 are added to activate Oxone® at low concentrations referring to the reported literature.[36] After the titration, EtBnS or *m*XyS derivatives were added to the solution. The reaction solution of EtBnS was submitted to NMR and LC-MS spectral measurements.

DFT calculations.

We optimized local minima on the potential energy surfaces using the unrestricted B3LYP method.[37] TD-DFT calculations were performed for 20 excited states on the basis of the optimized structures.[38] we used the LanL2TZ basis sets[39] for W, 6-31G* basis sets[40,41] for Co atom, and 6-31+G* basis sets[40,41] for O and P atoms. The Gaussian 09 (Revision C.01) program package[42] was used for all DFT calculations.

Notes and references

1 S. M. Arnold, J. Angerer, P. J. Boogaard, M. F. Hughes, R. B. O'Lone, S. H. Robison, A. R. Schnatter, *Crit. Rev. Toxicol.* 2013, **43**, 119–153.
2 S. H. Lamm, W. Grünwald, *Science* 2006, **312**, 998b–999b.
3 Luo, Y.-R. *Handbook of Bond Dissociation Energies in Organic Compounds*, 1st ed.; CRC Press LLC: Boca Raton, FL, 2003; p 39.
4 S. S. Tamhankar, K. Tsuchiya, J. B. Riggs, *Appl. Catal*. 1985, **16**, 103–121.
5 A. A. Dadkhah, A. Akgerman, *J. Hazard. Mater.* 2002, **B93**, 307–320.
6 D. A. Lashof, D. R. Ahuja, *Nature* 1990, **344**, 529–531.
7 C. Djerassi, R. R. Engle, *J. Am. Chem. Soc*. 1953, ***75***, 3838–3840.
8 J. A. Caputo, R. Fuchs, *Tetrahedron Lett.* 1967, **8**, 4729–4731.
9 R. Wojcieszak, F. Santarelli, S. Paul, F. Dumeignil, F. Cavani, R. V. Gonçalves, *Sustain. Chem. Process* 2015, **3**:9.
10 Y. Shimoyama, T. Ishizuka, H. Kotani, T. Kojima, *ACS Catal*. 2019, **9**, 671–678.
11 Y. Shimoyama, T. Ishizuka, H. Kotani, Y. Shiota, K. Yoshizawa, K. Mieda, T. Ogura, T. Okajima, S. Nozawa, T. Kojima, *Angew. Chem.*, *Int. Ed.* 2016, ***55***, 14041–14045.
12 D. Hong, J. Jung, J. Park, Y. Yamada, T. Suenobu, Y.-M. Lee, W. Nam, S. Fukuzumi. *Energy Environ. Sci.* 2012, **5**, 7606–7616.
13 S. S. Wang and G. Y. Yang, *Chem. Rev.*, 2015, **115**, 4893–4962.
14 I. A. Weinstock, R. E. Schreiber and R. Neumann, *Chem. Rev.*, 2018, **118**, 2680–2717.
15 M. Lechner, R. Güttel and C. Streb, *Dalton Trans.*, 2016, **45**, 16716–16726.
16 S. S. Balula, L. Cunha-Silva, I. C. M. S. Santos, A. C. Estrada, A. C. Fernandes, J. A. S. Cavaleiro, J. Pires, C. Freire, A. M. V. Cavaleiro, *New. J. Chem*. 2013, **37**, 2341–2350.
17 J. H. Choi, J. K. Kim, D. R. Park, T. H. Kang, J. H. Song, I. K. Song, *J. Mol. Cat. A: Chemical* 2013, **371**, 111–117.
18 S. J. Folkman, J. Soriano-Lopez, J. R. Galán-Mascarós, R. G. Finke, *J. Am. Chem. Soc*. 2018, **140**, 12040–12055.
19 C. M. Tourné, G. F. Tourné, *J. Inorg. Nucl. Chem*. 1970, **32**, 3875–3890.
20 (a) N. A. Alekar, S. Gopinathan, C. Gopinathan, *Indian J. Chem*. 2000, **39A**, 439–441. (b) J. Li, J. Wang, L. Zhang, X. Sang, W. You, *J. Coord. Chem*. 2017, **70**, 2950–2957.
21 In the ^{1}H NMR spectra, peroxidized species of EtBnS at the benzylic position was also observed and confirmed by *in-situ* reduction by sodium iodide. See Fig. S3 in the ESI.
22 M. E. González-Núñez, M. E. González-Núñez, R. Mello, A. Olmos, G. Asenisio, *J. Org. Chem.* 2005, **70**, 10879–10882.
23 The combination of cobalt(II) perchlorate salt and Oxone® affords a sulfate radical as a reactive species that can oxidise organic compounds. see ref: G. P. Anipsitakis, E. Stathatos, D. D. Dionysiou, *J. Phys. Chem. B*, 2005, **109**, 13052–13055.
24 S. B. Sinha, J. Campos, G. W. Brudvig, R. H. Crabtree, *RSC Adv*. 2014, **4**, 49395–49399.
25 M. Spiro, *Electrochem. Acta* 1979, **24**, 313–314.
26 L. Nurdin, D. M. Spasyuk, L. Fairburn, W. E. Piers, L. Maron, *J. Am. Chem. Soc.* 2018, **140**, 16094–16105.
27 E. Andris, R. Navrátil, J. Jasík, M. Srnec, M. Rodríguez, M. Costas, J. Roithová, *Angew. Chem.*, *Int. Ed*. 2019, **58**, 9619–9624.
28 Y. Shimoyama, T. Kojima, *Inorg. Chem.* 2019, **58**, 9517–9542.
29 The homolytic O-O bond cleavage of HSO_5^- or hydroperoxide ions coordinated to Co centre have been proposed in the following papers: (a) A. Ali, W. Akram, H.-Y. Liu, *Molecules*

View Article Online
DOI: 10.1039/D0CY01758B

2019, **24**, 78–94. (b) G. P. Anipsitakis, D. D. Dionysiou, *Environ. Sci. Technol.* 2003, **37**, 4790–4797. (c) I. Ilić, A. Milutinović-Nikolić, Z. Mojović, Z. Vuković, P. Vulić, I. Gržetić, P. Banković, N. Jović-Jovičić, *Appl. Clay Sci.* 2020, **193**, 105668.

30 R. Augusti, A. O. Dias, L. L. Rocha, R. M. Lago, *J. Phys. Chem. A* 1998, **102**, 10723–10727.

31 C. Hansch, A. Leo, R. W. Taft, *Chem. Rev*. 1991, **91**, 165–195.

32 T. Tsuji, A. A. Zaoputra, Y. Hitomi, K. Mieda, T. Ogura, Y. Shiota, K. Yoshizawa, H. Sato, M. Kodera, *Angew*. *Chem*., *Int. Ed*. 2017, **56**, 7779–7782.

33 B. T. Golding, M. L. Barnes, C. Bleasdale, A. P. Henderson, D. Jiang, X. Li, E. Mutlu, H. J. Petty, M. M. Sadeghi, *Chem.-Biol. Interact.* 2010, **184**, 196–200.

34 J. M. Carraher, T. Pfennig, R. G. Rao, B. H. Shanks, J.-P. Tessonnier, *Green Chem*. 2017, **19**, 3042–3050.

35 A. Courtin, H.-R. V. Tobel, P. Doswald, *Helv. Chim. Act*. 1978, **61**, 3079–3086.

36 J. F. Goodman, P. Robson, *J. Chem. Soc.* 1963, 2871–2875.

37 (a) A. D. Becke, *Phys. Rev. A* 1988, **38**, 3098–3100. (b) C. Lee, W. Yang, R. G. Part, *Phys. Rev. B* 1988, **37**, 785–789.

38 M. E. Casida, C. Jamorski, K. C. Casida, D. R. Salahub, *J. Chem. Phys*. 1998, **108**, 4439-4449.

39 P. J. Hay, W. R. Wadt, *J. Chem. Phys.* 1985, **82**, 299–310.

40 P. C. Hariharan, J. A. Pople, *Theoret. Chim. Acta* 1973, **28,** 213–222.

41 M. M. Francl, W. J. Pietro, W. J. Hehre, *J. Chem. Phys.* 1982, **77**, 3654–3665.

42 Gaussian 09, Revision C.01, M. J. Frisch, G. W. Trucks, H. B. Schlegel, G. E. Scuseria, M. A. Robb, J. R. Cheeseman, G. Scalmani, V. Barone, B. Mennucci, G. A. Petersson, H. Nakatsuji, M. Caricato, X. Li, H. P. Hratchian, A. F. Izmaylov, J. Bloino, G. Zheng, J. L. Sonnenberg, M. Hada, M. Ehara, K. Toyota, R. Fukuda, J. Hasegawa, M. Ishida, T. Nakajima, Y. Honda, O. Kitao, H. Nakai, T. Vreven, J. A. Montgomery, Jr., J. E. Peralta, F. Ogliaro, M. Bearpark, J. J. Heyd, E. Brothers, K. N. Kudin, V. N. Staroverov, T. Keith, R. Kobayashi, J. Normand, K. Raghavachari, A. Rendell, J. C. Burant, S. S. Iyengar, J. Tomasi, M. Cossi, N. Rega, J. M. Millam, M. Klene, J. E. Knox, J. B. Cross, V. Bakken, C. Adamo, J. Jaramillo, R. Gomperts, R. E. Stratmann, O. Yazyev, A. J. Austin, R. Cammi, C. Pomelli, J. W. Ochterski, R. L. Martin, K. Morokuma, V. G. Zakrzewski, G. A. Voth, P. Salvador, J. J. Dannenberg, S. Dapprich, A. D. Daniels, O. Farkas, J. B. Foresman, J. V. Ortiz, J. Cioslowski, and D. J. Fox, Gaussian, Inc., Wallingford CT, 2010.